




# Quantum Geometry and Many-Body Landau-Zener Tunneling in Time-dependent Quantum Systems with Instantaneous Quantum Integrability

Xiao Wang (王骁) <sup>1</sup>, Xiaodong He (何晓东) <sup>1</sup> and Jianda Wu (吴建达) <sup>1, 2, 3, \*</sup>

<sup>1</sup>*Tsung-Dao Lee Institute, Shanghai Jiao Tong University, Shanghai, 201210, China*

<sup>2</sup>*School of Physics & Astronomy, Shanghai Jiao Tong University, Shanghai, 200240, China*

<sup>3</sup>*Shanghai Branch, Hefei National Laboratory, Shanghai 201315, China*

We study quantum geometric effects in time-dependent quantum many-body systems quenched from integrable systems through a unitary transformation whose phase operator is linear in time. We establish a theorem stating that the Berry connection matrix thus all associated geometric quantities of the time-dependent many-body system, can be precisely characterized by excitations up to two-particle processes derived from the quantum integrable system. This geometric characterization provides a powerful lens for analyzing dynamical transitions in driven many-body settings. To illustrate the many-body geometric influence, we analyze a prototypical time-dependent Ising chain subjected to both a small longitudinal field and a slowly rotating transverse field, whose low-energy physics in the scaling limit is instantaneously governed by the quantum  $E_8$  integrable field theory. Focusing on the quantum geometric potential (QGP), we show the QGP continuously suppresses the instantaneous energy gaps with decreasing longitudinal field, thereby enhancing many-body Landau-Zener tunneling as evidenced by the Loschmidt echo and its associated spectral entropy. The critical threshold for the longitudinal field strength is determined, where the spectral entropy linearly increases with system size and exhibits hyperscaling behavior when approaching to the threshold. When the longitudinal field passes the threshold and decreases toward zero, the QGP continuously leads to vanishing instantaneous energy gaps involving more low-energy excitations, resulting in increasing spectral entropy indicative of many-body Landau-Zener tunneling. Our results unveil telltale quantum geometric signatures in time-dependent many-body systems, elucidating the intricate interplay between quantum geometry and dynamics.

## INTRODUCTION

Quantum geometric effects have attracted sustained research interests over the past several decades since the introduction of the Berry phase [1]. Significant progress has been made in fields such as topological band insulators [2–4], non-equilibrium adiabatic evolution [5, 6], and the quantum Hall effect [7]. For instance, the higher-order optical responses can be generally characterized by the Riemannian geometry of quantum states [2–4].

Despite the clear structure of quantum geometric quantities constructed from wavefunctions, studying quantum geometric effects in quantum many-body systems remains highly challenging, and related research is still scarce. This scarcity primarily stems from the complexity of many-body wavefunctions which involve an exponentially growing Hilbert space in such systems. For instance, calculating Berry connections in many-body systems poses significant challenges, both numerically and analytically.

Due to exact solvability, quantum integrable systems may provide critical insights into quantum geometry in many-body systems. For most quantum integrable systems, the eigenstates and corresponding transition matrix elements of physical observables can be calculated exactly using systematic methods, such as the Bethe Ansatz [8–17] or/and form factor bootstrap [18–22]. Over the past decade, significant research has focused on quantum integrability in non-equilibrium systems, including integrable quantum quenches and integrable brickwork

circuits [23–34]. These studies have provided new insights into non-equilibrium physics from the perspective of integrability, with potential connections to emerging fields such as quantum computing and quantum information. However, the understanding of quantum geometric effects in quantum many-body systems remains underdeveloped [35].

To study quantum geometry and its effects in quantum many-body systems, we focus on time-dependent many-body systems quenched from quantum integrable ones via a unitary transformation whose phase operator is linear in time with coefficient being sum/integral of (quasi)local operators. Apparently the unitary transformation keeps the system instantaneously integrable. Within these systems, we prove that the Berry connection matrix (BCM) entries  $\gamma_{nm} = i\langle\phi_n(t)|\dot{\phi}_m(t)\rangle$  only associate excitations up to two particle processes, where  $|\phi_n(t)\rangle$  is the  $n^{\text{th}}$  instantaneous eigenfunction with instantaneous eigenenergy  $e_n(t)$ .

For illustration we further consider the time evolution of a quantum Ising chain under both a slowly rotating transverse field and a small static longitudinal field [34, 36], where the initial state is set as the ground state at the beginning. We introduce a local U(1) gauge-invariant geometric term known as the quantum geometric potential (QGP)  $Q_{mn} = \gamma_{mm} - \gamma_{nn} + \frac{d}{dt}\arg \gamma_{nm}$  [37, 38] generated from any two instantaneous eigenfunctions. This term provides a crucial correction to the instantaneous energy gap  $e_{nm} = e_n(t) - e_m(t)$  and thus gives rise to a more efficient effective energy gap (EEG)

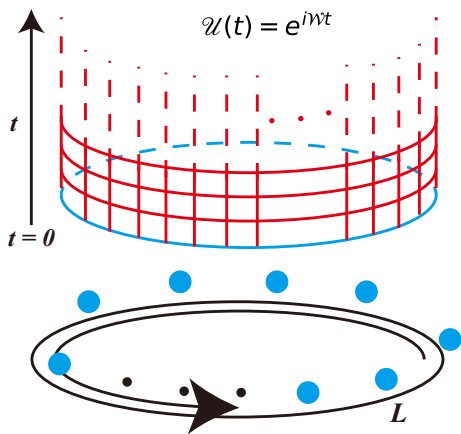


FIG. 1. An illustration of an eigenstate in an IFT containing  $n$  stable quasiparticles on a cylinder of a relatively large circumference  $L$ , and its time evolution process under  $\mathcal{U}(t) = e^{i\mathcal{W}t}$ .

$\Delta_{nm} = e_{nm} + Q_{mn}$ . Notably, even when the instantaneous energy gap  $e_{nm}$  is large, perfect Landau-Zener tunneling can still occur if the  $\Delta_{nm}$  vanishes when the QGP cancels the  $e_{nm}$ . This has been validated in the NMR experiment [39] and further demonstrated in time-dependent two-band models [5].

In the scaling limit, the QGP of this system can be analytically determined through the quantum  $E_8$  integrable field theory (IFT). The EEG can then be reduced to a more compact formalism as a function of the rotating frequency ( $\omega_0$ ) and the longitudinal field intensity ( $h_z$ ). We first identify our calculation of the QGP with the truncated conformal space approach (TCSA).

Then to show the influence of the QGP and EEG in many-body Landau-Zener tunneling (MBLZT) processes, we employ the truncated lattice free fermion approach (TLFFA) [40–43]. Within this framework, we analyze the spectral entropy of the Loschmidt echo (LE), which quantifies the overlap between the time-evolved wavefunction and the instantaneous ground state for different system sizes  $L$ . We find a critical  $\kappa \equiv h_z/(\omega_0/2)$ ,  $\kappa_c = 1$  which serves as a critical threshold for the MBLZT. When  $\kappa > 1$ , zeros of EEG are nearly absent, manifested as normal spectral entropy contributed from a limited number of finite-frequency modes. As  $\kappa$  goes to 1, a hyperscaling behavior of spectral entropy appears according to the scaling parameter  $(\kappa - 1)^{8/15}L$ . At  $\kappa = 1$ , the spectral entropy scales linearly with the system size  $L$ , implying MBLZT avalanche in thermodynamic limit. When  $\kappa \leq 1$  zeros of EEG substantially increase with decreasing  $\kappa$ , manifested as persistent growth of the LE spectral entropy, signaling significantly enhanced MBLZT. Interestingly, the LE spectral entropy also exhibits a cascade of additional peaks when  $\kappa \leq 1$ , where we expect strengthened MBLZT.

## THE BCM IN TIME-DEPENDENT SYSTEMS QUENCHED FROM QUANTUM INTEGRABLE SYSTEMS

It is generally difficult to calculate the BCM in interacting quantum many-body systems. However, if we consider a quenching process of an eigenstate in an IFT containing  $n$  stable quasiparticles,  $|\psi_n(t)\rangle = \mathcal{U}(t)|\psi_n\rangle_{\text{init},L} = e^{i\mathcal{W}t}|\psi_n\rangle_{\text{init},L}$ , where we have put this quantum field theory on a cylinder of a relatively large circumference  $L$ , with the unitary time evolution operator  $\mathcal{W}$  being an integration of local operator density  $\mathcal{W} = \int_0^L \mathcal{O}(x)dx$ . The initial state is given by  $|\psi_n\rangle_{\text{init},L} = |A_1(\vartheta_1; I_1) \dots A_N(\vartheta_N; I_N)\rangle_L$ . Here,  $A_j, j = 1, \dots, N$  label different types of particles with corresponding mass  $m_j$ , discrete quantum number  $I_j$ , and rapidity  $\vartheta_j$ . In addition, the energy and momentum of this state are given by  $E = \sum_j m_j \cosh \vartheta_j$  and  $P = \sum_j m_j \sinh \vartheta_j$ . For any single particle  $A_j(\vartheta_j; I_j)$ , the discrete momentum and rapidity are connected with each other by the Bethe-Yang quantization condition derived from the spatial periodic boundary condition [34, 40, 45–47]. An illustration is shown in Fig. 1. The BCM can then be explicitly given with the help of integrability. Considering two such states containing  $n$  and  $m$  quasiparticles respectively, for the off-diagonal matrix element  $m \neq n$ , the BCM is given by

$$\frac{\gamma_{nm}}{L} \approx -\frac{\mathcal{F}_{NM}^{\mathcal{O}}(\vartheta'_1 + i\pi, \dots, \vartheta'_N + i\pi, \vartheta_1, \dots, \vartheta_M)}{\sqrt{\rho_N(\vartheta'_1, \dots, \vartheta'_N)}\sqrt{\rho_M(\vartheta_1, \dots, \vartheta_M)}}, \quad (1)$$

with Lüscher's remainder  $o(e^{-\mu L})$  [45–48]. Here, the function  $\mathcal{F}_{nm}^{\mathcal{O}}$  in terms of rapidities is known as the form factor for certain IFT, and the  $\rho$  function comes from the Jacobian of the particle density of states determined by the Bethe-Yang condition. For the diagonal matrix element  $m = n$ , the result is given by

$$\frac{\gamma_{nn}}{L} \approx -_L\langle \mathcal{O} \rangle_L - \sum_{A \in \{A_1, \dots, A_N\}} \frac{\mathcal{F}_{NN}^{\mathcal{O}}(A)\rho(\{A_1, \dots, A_N\} \setminus A)_L}{\rho(\{A_1, \dots, A_N\})_L}, \quad (2)$$

with the Lüscher's remainder as well. The full information of the BCM implies that for such quantum many-body systems, we can determine all the geometric quantities associated with the BCM. Notably, the Jacobians in the denominator provide suppression behavior of order  $L^n$  with  $n$  being the number of particles involved. Consequently, after simple power counting, we can immediately observe that the excitations involving more than two particles do not contribute to the BCM in the thermodynamic limit ( $L \rightarrow \infty$ ). Thus we prove the following theorem.

**Theorem:** Consider a 1+1D time-dependent quantum many-body system with instantaneous quantum integrable

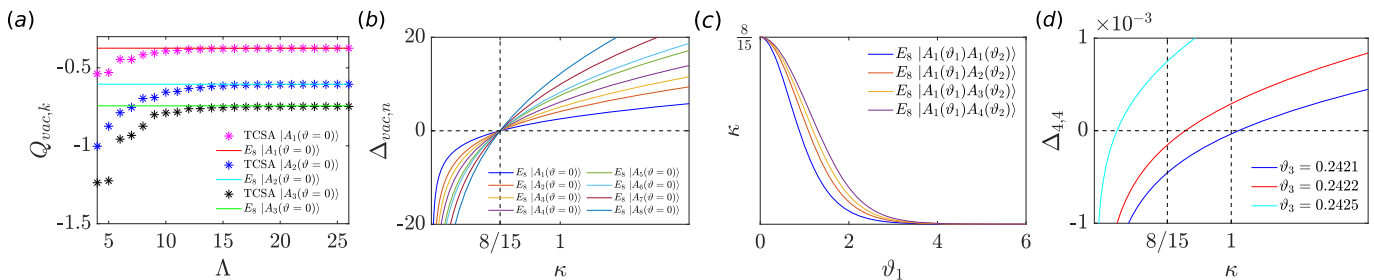


FIG. 2. (a) Comparison of the QGP between the ground state (vacuum of the  $\mathcal{H}_{E_8}$ ) and the three lightest single-particle states of the  $\mathcal{H}_{E_8}$ , calculated with both the  $\mathcal{H}_{E_8}$  form factor theory and the boosted TCSA algorithm [44]. Here,  $\Lambda$  is the truncation parameter satisfying  $E^2 - P^2 \leq \Lambda^2$ . (b) Analytical results of the EEG between the ground state and the 8 single  $E_8$  particle state with zero momentum, with  $0 < \kappa \leq 2$ . The zeros of EEG appear at  $\kappa = 8/15$  for all the single  $E_8$  particles. (c) The zeros of EEG as a function of  $A_1$ 's rapidity  $\vartheta_1$ , for the two-particle states  $A_1A_1$  to  $A_1A_4$ , with a zero momentum constraint  $m_i \sinh \vartheta_1 + m_j \sinh \vartheta_2 = 0$ . (d) Zeros of EEG between two four  $E_8$  particle states. While both the two groups of particles are of particle type  $A_{1\sim 4}$ , the rapidities for one of the states takes  $(\vartheta_1, \vartheta_2, \vartheta_3, \vartheta_4) = (0.2, 0.2, 0.1, 0.1)$ , and for the other one takes  $\vartheta_1 = \vartheta_2 = \vartheta_4 = 0.1$  and  $\vartheta_3 = 0.2421, 0.2422, 0.2425$ , corresponding to the zeros being from large to small, respectively.

bility, quenched from integrable systems, through a unitary transformation whose phase operator of the transformation is linear in time with coefficient being a sum of (quasi) local operators. In the thermodynamic limit, the BCM entries can be analytically obtained as excitations up to two particles.

In the following, the theorem is applied to a time-dependent quantum Ising model, where the QGP constructed from the BCM entries is shown to play a crucial role in the MBLZT in the system.

### A TIME-DEPENDENT QUANTUM ISING CHAIN WITH INSTANTANEOUS QUANTUM $E_8$ INTEGRABILITY

We start from a ferromagnetic Ising chain subjected to both a periodically rotating transverse field and a static longitudinal field [34, 36],

$$\mathcal{H}(t) = - \sum_{i=1}^L (\sigma_i^z \sigma_{i+1}^z + \cos \omega_0 t \sigma_i^x - \sin \omega_0 t \sigma_i^y + h_z \sigma_i^z), \quad (3)$$

with  $\hbar = c = 1$ , Pauli matrices  $\sigma_i^\alpha$  ( $\alpha = x, y, z$ ) at site  $i$ , the length of the chain  $L$ , and the neighboring spin coupling  $J = 1$ . Additionally, we require  $\omega_0, h_z \ll 1$ . It is not hard to observe that the Hamiltonian instantaneously appears as a quantum critical transverse-field Ising chain perturbed by a small longitudinal field, whose low-energy physics in the scaling limit is described by the quantum  $E_8$  IFT,

$$\mathcal{H}_{E_8} = \mathcal{H}_{c=1/2} - h \int \sigma(x) dx, \quad (4)$$

where  $\mathcal{H}_{c=1/2}$  is the central charge 1/2 conformal field theory,  $\sigma(x)$  is known as the spin density operator, and the coupling constant  $h$  gives an exact relation with the

mass of the lightest particle as  $m_1 = C_m h^{8/15}$ , with  $C_m = 4.4049\dots$ , and masses of all quantum  $E_8$  particles in units of  $m_1$  satisfy the eigenvalues of the Cartan matrix for  $E_8$  Lie algebra [21, 34, 49–51]. In the following we set the initial state  $|\psi(0)\rangle$  as the ground state of Eq. (3) at  $t = 0$ , which in the scaling limit is the vacuum state  $|0\rangle_h$  of the  $\mathcal{H}_{E_8}$ .

The general time-evolved wavefunction of the Hamiltonian Eq. (3) follows [34, 36]  $|\psi(t)\rangle = \mathcal{U}(t)^{-1} e^{-i\mathcal{H}_{\text{eff}}t} |\psi(0)\rangle$ , where the unitary transformation is given by  $\mathcal{U}(t) = \exp\{-\frac{i}{2}\omega_0 t \sum_i \sigma_i^z\}$ , satisfying  $\mathcal{U}(t)\mathcal{H}(t)\mathcal{U}(t)^{-1} = \mathcal{H}(t=0)$ , and the effective Hamiltonian  $\mathcal{H}_{\text{eff}} = \mathcal{U}\mathcal{H}(t)\mathcal{U}^{-1} + i\dot{\mathcal{U}}\mathcal{U}^{-1}$  follows,

$$\mathcal{H}_{\text{eff}} = - \sum_i \left[ \sigma_i^z \sigma_{i+1}^z + \sigma_i^x + (h_z - \frac{\omega_0}{2}) \sigma_i^z \right], \quad (5)$$

where for  $h_z \neq \omega_0/2$ , the low-energy physics is described by another  $\mathcal{H}_{E_8}$  with modified longitudinal coupling. Considering the instantaneous Schrödinger equation  $\mathcal{H}(t)|\psi_n(t)\rangle_{\text{ins}} = E_n(t)|\psi_n(t)\rangle_{\text{ins}}$ , where  $|\psi_n(t)\rangle_{\text{ins}}$  is the instantaneous eigenstate associated with the  $n^{\text{th}}$  instantaneous eigenenergy  $E_n(t)$ , it is straightforward to prove [40]  $E_n(t) = E_n(0)$  and  $|\psi_n(t)\rangle_{\text{ins}} = e^{i\varphi_n(t)} \mathcal{U}(t)^{-1} |\psi_n(0)\rangle$ , which implies that the instantaneous energy levels remain invariant for the Hamiltonian Eq. (3), and the instantaneous eigenstates are given by a global rotation according to  $\mathcal{U}(t)$  up to an additional time-dependent overall  $U(1)$  gauge  $\varphi_n(t)$ .

Now let's focus on the QGP  $Q_{mn}$ , taking the scaling limit of the model Eq. (3), the QGP follows

$$Q_{nm} = \sum_{j=1}^M \frac{\mathcal{F}_{jj}^{\mathcal{O}}(i\pi, 0)}{m_j \cosh \vartheta_j} - \sum_{i=1}^N \frac{\mathcal{F}_{ii}^{\mathcal{O}}(i\pi, 0)}{m_i \cosh \vartheta_i}. \quad (6)$$

As a concrete example, we consider the QGP between the vacuum state and the single  $E_8$  particle state with zero momentum, which is given by  $\mathcal{A}_{00} - \mathcal{A}_{kk} =$

$\langle \sigma \rangle \mathcal{F}_{kk}^\sigma(i\pi, 0)/m_k$  where  $\langle \sigma \rangle = C_\sigma h^{1/15}$  with  $C_\sigma = 1.27758 \dots$  [21, 34]. The results agree with those from the boosted TCSA algorithm [44], as shown in Fig. 2 (a) for  $k = 1, 2, 3$ .

### THE EEG IN TIME-DEPENDENT IFT

In the following we consider the EEG between two instantaneous eigenstates and try to find the zeros in  $\Delta_{mn}(t) = 0$  for any  $|\psi_m\rangle_{ins}$  and  $|\psi_n\rangle_{ins}$ . At the zeros, the quantum adiabatic condition is significantly violated [5, 37–39], and the MBLZT process shall occur. Moreover, when  $h_z$  decreases the EEG will cross zero and become negative, which suggests an effective swap of the high- and low-energy states instantaneously. Under this scenario, the MBLZT will be strongly enhanced because more and more higher-energy states effectively become low-energy due to the QGP. In the following we analytically solve the EEG for the "low-energy" sector of the Hamiltonian Eq. (3), whose results are associated with the  $\mathcal{H}_{E_8}$  [Eq. (4)].

In the scaling limit, for the low-energy sector the EEG during the time evolution can be solved analytically. Considering any two instantaneous eigenstates  $|\psi_n(t)\rangle_{ins}$  and  $|\psi_m(t)\rangle_{ins}$  in the model Eq. (3), the instantaneous energy gap reads  $E_{mn} = \sum_{\beta=1}^M m_\beta \cosh \theta_\beta - \sum_{\alpha=1}^N m_\alpha \cosh \theta'_\alpha$ , where we have assumed that there are totally  $M$  and  $N$  quantum  $E_8$  particles in the two states, respectively. With the mass ratios for the  $E_8$  particles  $\xi_i$  in units of  $m_1$ , the masses of the quantum  $E_8$  particles follows  $m_{\beta(\alpha)} = \xi_{\beta(\alpha)} m_1 = \xi_{\beta(\alpha)} C_m h_z^{8/15}$ , and  $\theta_{\beta(\alpha)}^{(\prime)}$  is the corresponding rapidity. The BCM entry is given by  $\gamma_{km}(t) = -\dot{\varphi}_m(t) \delta_{km} - \omega_0/2 \int dx \langle \psi_k | \sigma(x) | \psi_m \rangle$ . Applying the quantum  $E_8$  form factor theory, the QGP can be organized in a more compact form as [40]

$$Q_{nm}(t) = -\frac{8}{15\kappa} \left( \sum_{\beta=1}^M \frac{m_\beta}{\cosh \theta_\beta} - \sum_{\alpha=1}^N \frac{m_\alpha}{\cosh \theta'_\alpha} \right), \quad (7)$$

with  $\kappa \equiv h_z/(\omega_0/2)$  as introduced in the introduction. Thus the EEG finally reads

$$\Delta_{mn}(t) = \sum_{\beta=1}^M m_\beta \cosh \theta_\beta - \sum_{\alpha=1}^N m_\alpha \cosh \theta'_\alpha - \frac{8}{15\kappa} \left( \sum_{\beta=1}^M \frac{m_\beta}{\cosh \theta_\beta} - \sum_{\alpha=1}^N \frac{m_\alpha}{\cosh \theta'_\alpha} \right). \quad (8)$$

Interestingly, if taking one of the states being the ground state (vacuum) of the initial states, and the other one being the single particle state with zero momentum, the zeros of EEG are given by  $\kappa = 8/15$ , which does not depend on the type of the particles [*cf.* Fig. 2 (b)]. It is also

the upper bound for the zeros of EEG between the ground state and the higher excited states [40]. In the quantum  $E_8$  case, the higher excited states are readily given by single particle states with large rapidity (momentum) or multi-particle states. We show that for two-particle excitations with zero total momentum constraint, as one of the particles' rapidity goes to infinity, the corresponding zeros of the EEG will approach 0. It is also easy to verify from Eq. (8) that the zeros for two same particle combinations with zero total momentum will collapse to the same curve as  $A_1 A_1$ . The results are presented in Fig. 2 (c). However, if considering the zeros of EEG for any two instantaneous eigenstates, the region for zeros of EEG is beyond  $\kappa = 8/15$ . For instance, Fig. 2 (d) shows contribution of four-particle excitations to the EEG whose zeros appear to approach  $\kappa = 1$ .

### THE SPECTRAL ENTROPY OF THE LOSCHMIDT ECHO

In order to investigate the role of the EEG in the MBLZT process of a time-dependent quantum system, a commonly adopted approach is to examine the fidelity between the time-evolving wavefunction and the instantaneous eigenstates, denoted as  ${}_{ins} \langle \psi_n(t) | \psi(t) \rangle$ , which is known as the Loschmidt echo (LE).

For the time evolution governed by Eq. (3), the LE is expressed as  $\mathcal{L}_n(t) = \langle \psi_n(0) | e^{-i\mathcal{H}_{eff}t} | \psi(0) \rangle$ . Here, the index  $n$  is used to label the energy level of the corresponding excited states. When  $n$  corresponds to the ground state, we focus on the spectrum of the LE obtained through its Fourier transformation, which is given by  $\mathcal{L}_0(\omega) = \sum_m |\langle \phi_m | \psi_0 \rangle|^2 \delta(\omega - E_m)$ . Here,  $|\phi_m\rangle$  represents the eigenbasis of the  $\mathcal{H}_{eff}$ , and  $E_m$  is its corresponding eigenenergy. Detailed results for  $L = 80$  with different  $h_z$  from  $\omega_0/10$  to  $\omega_0$  are exhibited in [40]. To obtain a better understanding of the MBLZT, we introduce spectral entropy for the LE,

$$S_{LE} = - \sum_m p_m \ln p_m, \quad (9)$$

where  $p_m = |\langle \phi_m | \psi_0 \rangle|^2$ , and it naturally satisfies  $\sum_m p_m = 1$ . In the context of our study, the  $S_{LE}$  serves as a measure of the spectral density across the entire spectrum.

We use the TLFFA algorithm to calculate the quantities introduced above. The details of the TLFFA algorithm can be found in [40]. Specifically, in this algorithm, we truncate the free fermion basis to an energy of  $10J$  above the vacuum. For different system sizes, we ensure convergent results by increasing the number of states. For instance, for  $L = 100$  the number truncation of states reaches 16384 for convergence, and this also reaches our computational limit.

The results are summarized in Fig. 4. When  $\kappa \gg 1$ ,  $S_{LE}$  is small, indicating weak MBLZT. As  $\kappa$  decreases,  $S_{LE}$  increases continuously, suggesting an enhancement of MBLZT. When  $\kappa = 1$ , a peak appears and increases linearly in  $L$  [Fig. 4 inset (a)], which possibly implies MBLZT avalanche in thermodynamic limit. As  $\kappa$  decreases further below  $8/15$  upper bound of zeros of the EEG between the ground state and excited states, it is expected that the MBLZT is further strengthened, as manifested in the continuously increasing  $S_{LE}$ . Additional peaks appear when  $\kappa < 1$ , signaling further strengthened MBLZT at specific  $\kappa$ 's. For  $\kappa \rightarrow 0^+$ , it is noticed that the increase of  $S_{LE}$  becomes weaker for  $L = 100$  comparing to smaller  $L$  [Fig. 4 (b)], which possibly is due to the truncated energy cut at  $10J$  in our numerical calculation. A higher cut should provide better results, yet it exceeds our computational limit. Interestingly with  $\kappa$  approaching to 1,  $S_{LE}$  exhibits a hyperscaling behavior in terms of the scaling parameter  $(\kappa - 1)^{8/15} JL$  [Fig. 4 inset (b),  $J = 1$ ], implying emergence of universal physics near  $\kappa = 1$ .

The entire process can also be qualitatively understood in terms of the  $\mathcal{H}_{\text{eff}}$  [Eq. (5)]. Precisely at  $\kappa = 1$ , the  $\mathcal{H}_{\text{eff}}$  represents a quantum critical transverse field Ising chain with divergent density of states in the low energy sector, leading to a significant increase of the spectral entropy. When  $\kappa < 1$ , the spin alignment in the ground state of  $\mathcal{H}_{\text{eff}}$  is opposite to that of the initial ground state. This means that the initial state becomes a high-energy state with respect to the  $\mathcal{H}_{\text{eff}}$ , resulting in progressively stronger MBLZT as  $\kappa$  decreases.

## CONCLUSIONS

In this article we lay down a theorem revealing the quantum geometry in time-dependent many-body systems with instantaneous quantum integrability. The theorem demonstrates that the BCM elements in quenched integrable systems are governed by at most two-particle excitations. This result provides a geometric foundation for diabatic time evolutions mediated by the vanishing EEG due to the QGP contribution. We then analyze a time-dependent quantum Ising chain, showing that the suppression of the EEG with decreasing longitudinal field enhances the MBLZT. Near the critical ratio  $\kappa = 1$ , the hyperscaling behavior of the LE spectral entropy signals a sharp transition in the MBLZT. For  $\kappa < 1$ , the numerical results show persistent entropy growth mixing with a cascade of peaks, reflecting continuous enhancement of MBLZT. Our results indicate that the LE spectral entropy can serve as a powerful diagnostic tool for diabatic time evolution and its associated MBLZT. Yet, a full physical understanding on the analytical structure of the LE spectral entropy, such as its hyperscaling behavior, linear in  $L$  behavior at  $\kappa = 1$ , and additional peaks when

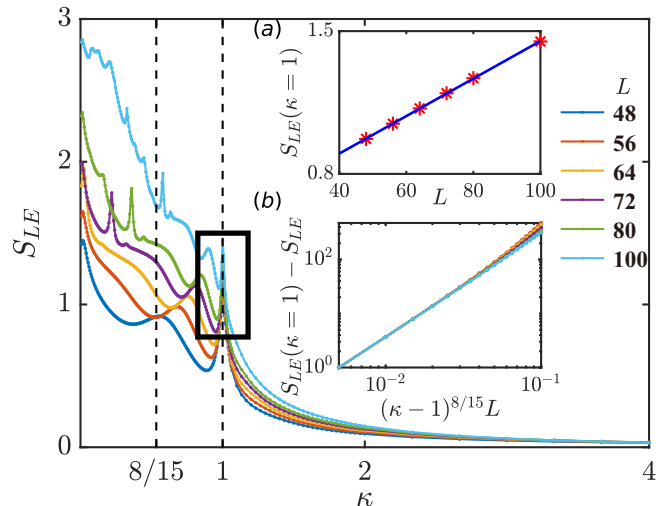


FIG. 3.  $S_{LE}$  vs.  $\kappa$  for different system sizes  $L$ 's. The  $S_{LE}$  at  $\kappa = 1$  linearly increases with  $L$  [inset (a)], along with more peaks emerging for  $\kappa \lesssim 8/15$ . When  $\kappa$  approaches 1, the  $S_{LE}$  collapses on the same curve for different  $L$  [inset (b)], implying hyperscaling behavior of  $S_{LE}$  w.r.t scaling parameter  $(\kappa - 1)^{8/15} L$ .

$\kappa < 1$ , requires more analytical and numerical efforts, a challenge that remains open but worth to explore further.

The time-dependent Hamiltonian in Eq. (3) is experimentally accessible in platforms such as Rydberg atomic arrays [34, 52, 53] which offer a promising setup for direct experimental verification of our theoretical predictions. Furthermore, our study reveals the important role of quantum geometry in time-dependent quantum many-body systems, providing an important insight into understanding non-equilibrium many-body systems.

## ACKNOWLEDGEMENTS

We thank Zongping Gong, Qicheng Tang, Thors Hans Hansson and Gabor Takács for helpful discussions. The TCSA calculation is supported by the TCSA package in [44]. The work is sponsored by National Natural Science Foundation of China Nos. 12274288, 12450004, the Innovation Program for Quantum Science and Technology Grant No. 2021ZD0301900, and the Tsung-Dao Lee Scholarship.

\* wujd@sjtu.edu.cn

- [1] B. M. Victor, Quantal phase factors accompanying adiabatic changes, *Proc. R. Soc. Lond. A* **392**, 45 (1984).
- [2] J. Ahn, G.-Y. Guo, and N. Nagaosa, Low-frequency divergence and quantum geometry of the bulk photovoltaic effect in topological semimetals, *Phys. Rev. X* **10**, 041041 (2020).

- [3] J. Ahn, G.-Y. Guo, N. Nagaosa, and A. Vishwanath, Riemannian geometry of resonant optical responses, *Nat. Phys.* **18**, 290 (2022).
- [4] Y.-S. Huang, Y.-H. Chan, and G.-Y. Guo, Large shift currents via in-gap and charge-neutral excitons in a monolayer and nanotubes of BN, *Phys. Rev. B* **108**, 075413 (2023).
- [5] S. Takayoshi, J. Wu, and T. Oka, Nonadiabatic nonlinear optics and quantum geometry - Application to the twisted Schwinger effect, *SciPost Phys.* **11**, 075 (2021).
- [6] T. Albash and D. A. Lidar, Adiabatic quantum computation, *Rev. Mod. Phys.* **90**, 015002 (2018).
- [7] D. J. Thouless, M. Kohmoto, M. P. Nightingale, and M. den Nijs, Quantized hall conductance in a two-dimensional periodic potential, *Phys. Rev. Lett.* **49**, 405 (1982).
- [8] E. H. Lieb and W. Liniger, Exact Analysis of an Interacting Bose Gas. I. The General Solution and the Ground State, *Phys. Rev.* **130**, 1605 (1963).
- [9] E. H. Lieb, Exact Analysis of an Interacting Bose Gas. II. The Excitation Spectrum, *Phys. Rev.* **130**, 1616 (1963).
- [10] M. Gaudin, Un système a une dimension de fermions en interaction, *Phys. Lett. A* **24**, 55 (1967).
- [11] C. N. Yang, Some exact results for the many-body problem in one dimension with repulsive delta-function interaction, *Phys. Rev. Lett.* **19**, 1312 (1967).
- [12] M. Jimbo and T. Miwa, *Algebraic Analysis of Solvable Lattice Models* (American Mathematical Society, 1995).
- [13] X.-W. Guan, M. T. Batchelor, and C. Lee, Fermi gases in one dimension: From Bethe ansatz to experiments, *Rev. Mod. Phys.* **85**, 1633 (2013).
- [14] F. He, Y. Jiang, Y.-C. Yu, H.-Q. Lin, and X.-W. Guan, Quantum criticality of spinons, *Phys. Rev. B* **96**, 220401 (2017).
- [15] F. Franchini, *An Introduction to Integrable Techniques for One-Dimensional Quantum Systems*, Vol. 940 (Springer, Cham, 2017).
- [16] J. Yang, X. Wang, and J. Wu, Magnetic excitations in the one-dimensional Heisenberg-Ising model with external fields and their experimental realizations, *J. Phys. A: Math. Theor.* **56**, 013001 (2023).
- [17] J. Yang and J. Wu, Truncated string state space approach and its application to the nonintegrable spin- $\frac{1}{2}$  Heisenberg chain, *Phys. Rev. B* **109**, 214421 (2024).
- [18] F. A. Smirnov, *Form Factors in Completely Integrable Models of Quantum Field Theory* (World Scientific, 1992).
- [19] V. E. Korepin, N. M. Bogoliubov, and A. G. Izergin, *Quantum Inverse Scattering Method and Correlation Functions* (Cambridge University Press, 1993).
- [20] B. Sutherland, *Beautiful Models* (World Scientific, 2004).
- [21] G. Delfino and G. Mussardo, The spin-spin correlation function in the two-dimensional ising model in a magnetic field at  $T = T_c$ , *Nucl. Phys. B* **455**, 724 (1995).
- [22] K. Hódsági and M. Kormos, Kibble-zurek mechanism in the Ising Field Theory, *SciPost Phys.* **9**, 055 (2020).
- [23] G. Delfino, Quantum quenches with integrable pre-quench dynamics, *J. Phys. A: Math. Theor.* **47**, 402001 (2014).
- [24] G. Delfino and M. Sorba, On unitary time evolution out of equilibrium, *Nucl. Phys. B* **1005**, 116587 (2024).
- [25] J.-S. Caux and F. H. L. Essler, Time evolution of local observables after quenching to an integrable model, *Phys. Rev. Lett.* **110**, 257203 (2013).
- [26] P. Calabrese, F. H. L. Essler, and M. Fagotti, Quantum quench in the transverse-field Ising chain, *Phys. Rev. Lett.* **106**, 227203 (2011).
- [27] M. Kormos, M. Collura, G. Takács, and P. Calabrese, Real-time confinement following a quantum quench to a non-integrable model, *Nat. Phys.* **13**, 246 (2017).
- [28] G. Delfino and J. Viti, On the theory of quantum quenches in near-critical systems, *J. Phys. A: Math. Theor.* **50**, 084004 (2017).
- [29] K. Hódsági, M. Kormos, and G. Takács, Quench dynamics of the Ising field theory in a magnetic field, *SciPost Phys.* **5**, 027 (2018).
- [30] E. Granet, M. Fagotti, and F. H. L. Essler, Finite temperature and quench dynamics in the Transverse Field Ising Model from form factor expansions, *SciPost Phys.* **9**, 033 (2020).
- [31] M. Vanicat, L. Zadnik, and T. c. v. Prosen, Integrable trotterization: Local conservation laws and boundary driving, *Phys. Rev. Lett.* **121**, 030606 (2018).
- [32] E. Vernier, B. Bertini, G. Giudici, and L. Piroli, Integrable digital quantum simulation: Generalized gibbs ensembles and trotter transitions, *Phys. Rev. Lett.* **130**, 260401 (2023).
- [33] A. Hutsalyuk, Y. Jiang, B. Pozsgay, H. Xu, and Y. Zhang, Exact spin correlators of integrable quantum circuits from algebraic geometry, [arXiv:2405.16070](https://arxiv.org/abs/2405.16070) (2024).
- [34] X. Wang, M. Oshikawa, M. Kormos, and J. Wu, Magnetization oscillations in a periodically driven transverse field Ising chain, *Phys. Rev. B* **110**, 195101 (2024).
- [35] V. V. Bazhanov, V. V. Mangazeev, and S. M. Sergeev, Quantum geometry of three-dimensional lattices, *J. Stat. Mech.* **2008**, P07004 (2008).
- [36] N. J. Robinson, I. P. Castillo, and E. Guzmán-González, Quantum quench in a driven Ising chain, *Phys. Rev. B* **103**, L140407 (2021).
- [37] J.-d. Wu, M.-s. Zhao, J.-l. Chen, and Y.-d. Zhang, Adiabatic condition and quantum geometric potential, *Phys. Rev. A* **77**, 062114 (2008).
- [38] C. Xu, J. Wu, and C. Wu, Quantized interlevel character in quantum systems, *Phys. Rev. A* **97**, 032124 (2018).
- [39] J. Du, L. Hu, Y. Wang, J. Wu, M. Zhao, and D. Suter, Experimental study of the validity of quantitative conditions in the quantum adiabatic theorem, *Phys. Rev. Lett.* **101**, 060403 (2008).
- [40] See Supplemental Material at [URL will be inserted by publisher] for details.
- [41] N. Iorgov, V. Shadura, and Y. Tykhyy, Spin operator matrix elements in the quantum Ising chain: fermion approach, *J. Stat. Mech.* , P02028 (2011).
- [42] V. Yurov and A. Zamolodchikov, Truncated-fermionic-space approach to the critical 2d ising model with magnetic field, *Int. J. Mod. Phys. A* **06**, 4557 (1990).
- [43] N. Albert, Y. Zhang, and H.-H. Tu, Truncated gaussian basis approach for simulating many-body dynamics, [arXiv:2410.04204](https://arxiv.org/abs/2410.04204) (2024).
- [44] H. Chen, A. L. Fitzpatrick, E. Katz, and Y. Xin, Giving hamiltonian truncation a boost, [arXiv:2207.01659](https://arxiv.org/abs/2207.01659) (2022).
- [45] B. Pozsgay and G. Takács, Form factors in finite volume I: Form factor bootstrap and truncated conformal space, *Nucl. Phys. B* **788**, 167 (2008).
- [46] B. Pozsgay and G. Takács, Form factors in finite volume II: Disconnected terms and finite temperature correla-

- tors, *Nucl. Phys. B* **788**, 209 (2008).
- [47] K. Hódsági, M. Kormos, and G. Takács, Perturbative post-quench overlaps in quantum field theory, *J. High Energy Phys.* (8).
- [48] M. Lüscher, Volume dependence of the energy spectrum in massive quantum field theories, I. stable particle states, *Commun. Math. Phys.* **104**, 177 (1986).
- [49] V. Fateev, The exact relations between the coupling constants and the masses of particles for the integrable perturbed conformal field theories, *Phys. Lett. B* **324**, 45 (1994).
- [50] X. Wang, H. Zou, K. Hódsági, M. Kormos, G. Takács, and J. Wu, Cascade of singularities in the spin dynamics of a perturbed quantum critical Ising chain, *Phys. Rev. B* **103**, 235117 (2021).
- [51] X. Wang, K. Puzniak, K. Schmalzl, C. Balz, M. Matsuda, A. Okutani, M. Hagiwara, J. Ma, J. Wu, and B. Lake, Spin dynamics of the  $E_8$  particles, *Science Bulletin* **69**, 2974 (2024).
- [52] C. Monroe, W. C. Campbell, L.-M. Duan, Z.-X. Gong, A. V. Gorshkov, P. W. Hess, R. Islam, K. Kim, N. M. Linke, G. Pagano, P. Richerme, C. Senko, and N. Y. Yao, Programmable quantum simulations of spin systems with trapped ions, *Rev. Mod. Phys.* **93**, 025001 (2021).
- [53] J. Wurtz, A. Bylinskii, B. Braverman, J. Amato-Grill, S. H. Cantu, F. Huber, A. Lukin, F. Liu, P. Weinberg, J. Long, S.-T. Wang, N. Gemelke, and A. Keesling, Aquila: Quera's 256-qubit neutral-atom quantum computer, [arXiv:2306.11727](https://arxiv.org/abs/2306.11727) (2023).
- [54] P. Fonseca and A. Zamolodchikov, Ising field theory in a magnetic field: Analytic properties of the free energy, *J. Stat. Phys.* (2003).
- [55] P. Pfeuty, The one-dimensional ising model with a transverse field, *Ann. Phys.* **59**, 79 (1970).
- [56] S. Sachdev, *Quantum Phase Transitions* (Cambridge University Press, Cambridge, England, 2011) pp. 1–521.

## Supplemental Material—Quantum Geometry and Many-Body Landau-Zener Tunneling in Time-dependent Quantum Systems with Instantaneous Quantum Integrability

### A. Finite Size formalism for Integrable Field Theory

In this section, we briefly introduce the framework of integrable field theory (IFT) that is defined on a cylinder with a sufficiently large spatial length  $L$ , while time ranges from  $-\infty$  to  $+\infty$ . The formalism has been well developed by B. Pozsgay and G. Takács, and more detailed reviews can be found in [45–47]. The asymptotic free multi-particle state for an infinite IFT is denoted by the particle species and their corresponding rapidities, as

$$|\psi_N\rangle = |A_{a_1}(\vartheta_1)\dots A_{a_N}(\vartheta_N)\rangle, \quad (10)$$

with the normalization as  $\langle A_{a_i}(\theta_i)|A_{a_j}(\theta_j)\rangle = 2\pi\delta_{a_i a_j}\delta(\theta_i - \theta_j)$ . In the finite size framework, such multi-particle states are relabeled with the quantum numbers as

$$|\psi_N\rangle_L = |A_{a_1}(I_1)\dots A_{a_N}(I_N)\rangle_L, \quad (11)$$

with the normalization as  $\langle A_{a_i}(I_i)|A_{a_j}(I_j)\rangle = \delta_{a_i a_j}\delta_{I_i I_j}$ . Due to the periodic boundary conditions, the quantum numbers are connected with the rapidities via the Bethe-Yang equation from the finite size field theory scheme,

$$m_i L \sinh \theta_i - i \sum_{j \neq i} \ln S_{ij}(\theta_i - \theta_j) = 2\pi I_i = Q_i, \quad (12)$$

with  $S_{ij}(\theta_i - \theta_j)$  being the corresponding scattering matrix. However, it is clearly observed that there is a measure difference between the normalizations of the two quantum states. Thus all the related quantities such as the complete basis and form factors (FF) will be influenced. This issue can be done by introducing the Jacobian given by the corresponding particle sets,

$$\rho_{a_1, \dots, a_n}(\theta_1, \dots, \theta_n) = \text{Det} \left( \frac{\partial Q_k(\theta_1, \dots, \theta_n)}{\partial \theta_l} \right), \quad (13)$$

and we have the following measure transformation between all the associated quantities,

$$\begin{aligned} \langle 0|\mathcal{O}|A_{a_1}(I_1)\dots A_{a_N}(I_N)\rangle_L &= \frac{F_n^\mathcal{O}(\theta_1, \dots, \theta_n)_{a_1, \dots, a_n}}{\sqrt{\rho_{a_1, \dots, a_n}(\theta_1, \dots, \theta_n)}}, \\ |A_{a_1}(I_1)\dots A_{a_N}(I_N)\rangle_L &= \frac{|A_{a_1}(\theta_1)\dots A_{a_N}(\theta_N)\rangle}{\sqrt{\rho_{a_1, \dots, a_n}(\theta_1, \dots, \theta_n)}}, \\ \sum_{I_1, \dots, I_n} &= \int \frac{d\theta_1 \dots d\theta_n}{(2\pi)^n} \rho_{a_1, \dots, a_n}(\theta_1, \dots, \theta_n), \end{aligned} \quad (14)$$

where  $F_n^\mathcal{O}(\theta_1, \dots, \theta_n)_{a_1, \dots, a_n} = \langle 0|\mathcal{O}|A_{a_1}(\theta_1)\dots A_{a_n}(\theta_n)\rangle$  is known as the FF for operator  $\mathcal{O}$ .

## B. A proof to the theorem

This section gives the proof of the theorem in the main text. Considering a quenched process of an eigenstate in an IFT containing  $n$  stable quasiparticles,

$$|\psi_n(t)\rangle = \mathcal{W}(t)|\psi_n\rangle_{\text{init},L} = e^{i\mathcal{W}t}|\psi_n\rangle_{\text{init},L}, \quad (15)$$

where we have put this quantum field theory on a cylinder with circumference  $L$ , with the unitary time evolution operator  $\mathcal{W}$  being an integration of local operator density

$$\mathcal{W} = \int_0^L \mathcal{O}(x)dx. \quad (16)$$

The initial state is given by

$$|\psi_n\rangle_{\text{init},L} = |A_1(\vartheta_1; I_1) \dots A_N(\vartheta_N; I_N)\rangle_L. \quad (17)$$

The related parameters have been introduced in the main text. According to the definition of the Berry connections, we focus on calculating the quantities  $\gamma_{nm} = i\langle\psi_n(t)|\dot{\psi}_m(t)\rangle$ . Introducing  $|\psi_m(t)\rangle$  with  $M$  stable quasi-particles, then we have [47]

$$\gamma_{nm} = -\langle\psi_n|\mathcal{W}|\psi_m\rangle = -L\langle\psi_n|\mathcal{O}|\psi_m\rangle_{p_{\psi_n}=p_{\psi_m}}, \quad (18)$$

where  $p_{\psi_n}$  and  $p_{\psi_m}$  are the total momentum of the corresponding quantum states. Using the framework listed in Sec. A, for the off-diagonal matrix element  $n \neq m$ , we have

$$\langle\psi_n|\mathcal{O}|\psi_m\rangle = {}_L\langle A_1(\vartheta'_1; I'_1) \dots A_N(\vartheta'_N; I'_N)|\mathcal{O}|A_1(\vartheta_1; I_1) \dots A_M(\vartheta_M; I_M)\rangle_L = \frac{\mathcal{F}_{NM}^{\mathcal{O}}(\vartheta'_1 + i\pi, \dots, \vartheta'_N + i\pi, \vartheta_1, \dots, \vartheta_M)}{\sqrt{\rho_N(\vartheta'_1, \dots, \vartheta'_N)}\sqrt{\rho_M(\vartheta_1, \dots, \vartheta_M)}}, \quad (19)$$

More interestingly, for the diagonal matrix element, in the infinite IFT if we recall the kinematic singularities of the form factor [21, 34, 47, 50],

$$-i \lim_{\theta_a \rightarrow \theta_b} (\theta_a - \theta_b) F_{a,b,a_1, \dots, a_n}^{\mathcal{O}}(\theta_a + i\pi, \theta_b, \theta_{a_1}, \dots, \theta_{a_n}) = \left(1 - \prod_n S_{b,a_i}(\theta_b - \theta_{a_i})\right) F_{a_1, \dots, a_n}^{\mathcal{O}}(\theta_{a_1}, \dots, \theta_{a_n}), \quad (20)$$

a divergence will always appear in such matrix element [while though it is possible to observe such divergence in Eq. (19), the density of states for such divergent off-diagonal items are extremely small]. A way to correctly recover such divergence in the finite size framework of IFT is developed in [45–47], which follows,

$${}_L\langle A_1(\vartheta_1; I_1) \dots A_M(\vartheta_M; I_M)|\mathcal{O}|A_1(\vartheta_1; I_1) \dots A_M(\vartheta_M; I_M)\rangle_L \approx {}_L\langle\mathcal{O}\rangle_L + \sum_{A \in \{A_1, \dots, A_N\}} \frac{\mathcal{F}_{NN}^{\mathcal{O}}(A)\rho(\{A_1, \dots, A_N\} \setminus A)_L}{\rho(\{A_1, \dots, A_N\})_L}, \quad (21)$$

where  $A$  is particle set contains particles with types  $a_1$  to  $a_M$ ,  $\mathcal{F}$  is FF corresponding to particle set  $A$ , By making use of Eq. (19) and Eq. (21), we obtain the results for the Berry connection matrix entries. For the off-diagonal matrix entries  $m \neq n$ ,

$$\frac{\gamma_{nm}}{L} \approx -\frac{\mathcal{F}_{NM}^{\mathcal{O}}(\vartheta'_1 + i\pi, \dots, \vartheta'_N + i\pi, \vartheta_1, \dots, \vartheta_M)}{\sqrt{\rho_N(\vartheta'_1, \dots, \vartheta'_N)}\sqrt{\rho_M(\vartheta_1, \dots, \vartheta_M)}}. \quad (22)$$

For the diagonal matrix elements  $m = n$ ,

$$\frac{\gamma_{nn}}{L} \approx -{}_L\langle\mathcal{O}\rangle_L - \sum_{A \in \{A_1, \dots, A_N\}} \frac{\mathcal{F}_{NN}^{\mathcal{O}}(A)\rho(\{A_1, \dots, A_N\} \setminus A)_L}{\rho(\{A_1, \dots, A_N\})_L}, \quad (23)$$

as shown in the main text. Noticing that the Jacobian Eq. (13) is a polynomial of order  $L^M$ , it is easy to see that in Eq. (22) only the term that  $(M+N)/2 \leq 1$  [as in Eq. (23) only the term that  $N \leq 1$ ] finally survives in the thermodynamic limit, suggesting that the contributions for the Berry connection matrix elements are up to two particle excitations.



### C. The instantaneous energy levels and eigenstates

We investigate the instantaneous Schrödinger equation  $\mathcal{H}(t)|\psi_n(t)\rangle_{ins} = E_n(t)|\psi_n(t)\rangle_{ins}$  for the following Hamiltonian,

$$\mathcal{H}(t) = -J \sum_{i=1}^L (\sigma_i^z \sigma_{i+1}^z + \cos \omega_0 t \sigma_i^x - \sin \omega_0 t \sigma_i^y + h_z \sigma_i^z). \quad (24)$$

Under the unitary transformation  $\mathcal{U}(t) = \exp \left\{ -\frac{i}{2} \omega_0 t \sum_i \sigma_i^z \right\}$ , we have [34, 36]

$$\mathcal{U}(t) \mathcal{H}(t) \mathcal{U}(t)^{-1} = -J \sum_{i=1}^L (\sigma_i^z \sigma_{i+1}^z + \sigma_i^x + h_z \sigma_i^z) = \mathcal{H}_{t=0}. \quad (25)$$

Applying the eigenstate of  $\mathcal{H}_{t=0}$  on both side,

$$\mathcal{U}(t) \mathcal{H}(t) \mathcal{U}(t)^{-1} |\psi_n(0)\rangle = \mathcal{H}_{t=0} |\psi_n(0)\rangle = E_n |\psi_n(0)\rangle, \quad (26)$$

and this further gives

$$\mathcal{H}(t) \mathcal{U}(t)^{-1} |\psi_n(0)\rangle = E_n \mathcal{U}(t)^{-1} |\psi_n(0)\rangle, \quad (27)$$

i.e., the instantaneous eigenstate  $|\psi_n(t)\rangle_{ins}$  is proportional to  $\mathcal{U}(t)^{-1} |\psi_n(0)\rangle$  while they have the same time-independent eigenenergy  $E_n$ . Without loss of generality, we conclude

$$E_n(t) = E_n(0), \quad |\psi_n(t)\rangle_{ins} = e^{i\varphi_n(t)} \mathcal{U}(t)^{-1} |\psi_n(0)\rangle, \quad (28)$$

with  $\varphi_n(t)$  being a time-dependent U(1) gauge.

### D. Calculation of the quantum geometric potential

The effective energy gap is defined as  $\Delta_{mn}(t) = E_m(t) - E_n(t) + Q_{nm}(t)$ , where  $E_{m,n}(t)$  are the instantaneous eigenenergy of the corresponding states, and

$$Q_{nm}(t) = \gamma_{nn}(t) - \gamma_{mm}(t) + \frac{d}{dt} \arg \left[ \langle \psi_m(t) | \dot{\psi}_n(t) \rangle \right]_{ins} \quad (29)$$

is known as the quantum geometric potential (QGP), with  $\gamma_{nn}(t) = {}_{ins} \langle \dot{\psi}_n(t) | \psi_n(t) \rangle_{ins}$  being the Berry connection [5, 37, 38]. We consider the effective energy gap between any two arbitrary excited states, which in the scaling limit corresponds to two multi- $E_8$  particle states containing  $N$  and  $M$  quantum  $E_8$  particles, respectively. The instantaneous energy gap is proven to be static, and can be directly read as

$$E_m(t) - E_n(t) = \sum_{\beta=1}^M m_\beta \cosh \theta_\beta - \sum_{\alpha=1}^N m_\alpha \cosh \theta'_\alpha. \quad (30)$$

On the lattice, using Eq. (28), the Berry connection is given by

$$\begin{aligned} \gamma_{mm}(t) &= -\dot{\varphi}_m(t) - \frac{\omega_0}{2} \sum_{i=1}^L \langle \psi_m(0) | \sigma_i^z | \psi_m(0) \rangle, \\ \gamma_{nn}(t) &= -\dot{\varphi}_n(t) - \frac{\omega_0}{2} \sum_{i=1}^L \langle \psi_n(0) | \sigma_i^z | \psi_n(0) \rangle. \end{aligned} \quad (31)$$

Since we also have

$$\frac{d}{dt} \arg \left[ \langle \psi_m(t) | \dot{\psi}_n(t) \rangle \right]_{ins} = \dot{\varphi}_n(t) - \dot{\varphi}_m(t). \quad (32)$$

The QGP is given as following,

$$Q_{nm}(t) = \frac{\omega_0}{2} \sum_{i=1}^L (\langle \psi_m(0) | \sigma_i^z | \psi_m(0) \rangle - \langle \psi_n(0) | \sigma_i^z | \psi_n(0) \rangle), \quad (33)$$

which also implies that the QGP is U(1) gauge invariant. To obtain the exact expression of the QGP, we use the finite size field theory frame and the results in Sec. A and B [45–47]. We first transform the system into the scaling limit. Since  $\langle \sigma \rangle = \bar{s} J^{1/8} \langle \sigma^z \rangle$  [34, 54],

$$Q_{nm}^s = \frac{\omega}{2} \bar{s}^{-1} J^{-1/8} \lim_{L \rightarrow \infty} 2JL ({}_L \langle \theta_1 \dots \theta_M | \sigma | \theta_1 \dots \theta_M \rangle_L - {}_L \langle \theta'_1 \dots \theta'_N | \sigma | \theta'_1 \dots \theta'_N \rangle_L), \quad (34)$$

with  $\omega$  being the scaling limit of  $\omega_0$ ,  $L = Na$  being the length of the system, and  $a$  being the lattice spacing, satisfying  $2Ja = \hbar c = 1$  [21, 50]. Introducing the general FF for the quantum  $E_8$  field theory,

$$F_{a_1, \dots, a_n, b_1, \dots, b_m}^{\mathcal{O}}(\theta_1, \dots, \theta_n, \theta_{n+1}, \dots, \theta_{n+m}) = {}_{a_1, \dots, a_n} \langle \theta_1, \dots, \theta_n | \mathcal{O} | \theta_{n+1}, \dots, \theta_{n+m} \rangle_{b_1, \dots, b_m} / \langle \mathcal{O} \rangle. \quad (35)$$

The  $E_8$  FF theory and a complete FF bootstrapping process can be found in Refs. [21, 47, 50]. According to previous analysis of the FFs, the QGP follows,

$$Q_{nm}^s(t) = \frac{\omega}{2} \bar{s}^{-1} J^{-1/8} \langle \sigma \rangle 2J \left( \sum_{\beta=1}^M \frac{F_{\beta\beta}^\sigma(i\pi, 0)}{m_\beta \cosh \theta_\beta} - \sum_{\alpha=1}^N \frac{F_{\alpha\alpha}^\sigma(i\pi, 0)}{m_\alpha \cosh \theta'_\alpha} \right). \quad (36)$$

This result implies that the QGP for this system is only related with the diagonal two-particle FFs in quantum  $E_8$  field theory. In fact, it can be further reduced to a more transparent form. Since  $m_\beta = C_m^s h^{8/15} e_\beta$ , with  $e_\beta$  being the Cartan roots of  $E_8$  exceptional Lie algebra,  $\langle \sigma \rangle = C_\sigma^s h^{1/15}$ , with  $h$  being  $h_z$  in the scaling limit, and  $C_\sigma^s = 4(C_m^s)^2/15\varphi_{11}$ , where  $\varphi_{11}$  is a constant [21], we can obtain that,

$$\begin{aligned} Q_{nm}^s(t) &= \frac{\omega}{2} \bar{s}^{-1} J^{-1/8} \langle \sigma \rangle 2J \left( \sum_{\beta=1}^M \frac{F_{\beta\beta}^\sigma(i\pi, 0)}{m_\beta \cosh \theta_\beta} - \sum_{\alpha=1}^N \frac{F_{\alpha\alpha}^\sigma(i\pi, 0)}{m_\alpha \cosh \theta'_\alpha} \right) \\ &= \frac{\omega}{2} \frac{4C_m^s}{15\varphi_{11}} \bar{s}^{-1} J^{-1/8} 2J h^{-7/15} \left( \sum_{\beta=1}^M \frac{F_{\beta\beta}^\sigma(i\pi, 0)}{m_\beta \cosh \theta_\beta} - \sum_{\alpha=1}^N \frac{F_{\alpha\alpha}^\sigma(i\pi, 0)}{m_\alpha \cosh \theta'_\alpha} \right). \end{aligned} \quad (37)$$

It can be proven that  $F_{\beta\beta}^\sigma(i\pi, 0)/e_\beta^2 = -2\varphi_{11}$ , which is not related with specific particle type. For showing this, we consider the trace of the stress-energy tensor  $\Theta(x)$  [21],

$$\langle m_\beta | \Theta(x) | m_\beta \rangle = 2\pi m_\beta^2 = 2\pi (C_m^s)^2 h^{16/15} e_\beta^2. \quad (38)$$

On the other hand, since  $\Theta(x) = 2\pi h(2 - 2\Delta_\sigma)\sigma(x)$ , where  $\Delta_\sigma = 1/16$  is the conformal weight of  $\sigma(x)$ , together with  $C_\sigma^s = 4(C_m^s)^2/15\varphi_{11}$ , we can immediately obtain that  $F_{\beta\beta}^\sigma(i\pi, 0)/e_\beta^2 = -2\varphi_{11}$ . Then the QGP is further reduced as

$$Q_{nm}^s(t) = -\frac{\omega}{2} \frac{8}{15h} \bar{s}^{-1} J^{-1/8} 2J \left( \sum_{\beta=1}^M \frac{m_\beta}{\cosh \theta_\beta} - \sum_{\alpha=1}^N \frac{m_\alpha}{\cosh \theta'_\alpha} \right). \quad (39)$$

Sending back to the lattice limit, using  $h = 2J^{15/8} h_z / \bar{s}$  [34, 50], we finally obtain that

$$Q_{nm}(t) = -\frac{\omega_0}{2J} \frac{8}{15h_z} \left( \sum_{\beta=1}^M \frac{m_\beta}{\cosh \theta_\beta} - \sum_{\alpha=1}^N \frac{m_\alpha}{\cosh \theta'_\alpha} \right). \quad (40)$$

This implies that the QGPs in this system are only related with the contributions from all the quantum  $E_8$  particles in the corresponding quantum  $E_8$  states.

### E. Technical Details of TLFFA

We provide additional details about the truncated lattice free fermion approach (TLFFA). Given the Hamiltonian

$$\mathcal{H} = \mathcal{H}_0 - Jh_z \sum_{i=1}^L \sigma_i^z, \quad (41)$$

where  $\mathcal{H}_0$  represents the Hamiltonian of the transverse field Ising chain with periodic boundary condition,

$$\mathcal{H}_0 = -J \sum_{i=1}^L (\sigma_i^z \sigma_{i+1}^z + g \sigma_i^x). \quad (42)$$

To construct the Hamiltonian for TLFFA, we introduce the dual Jordan-Wigner (JW) transformation [41]. The usual JW transformation is given by [55, 56]

$$\sigma_i^z = \prod_{i' < i} (1 - 2c_{i'}^\dagger c_{i'}) (c_i^\dagger + c_i), \quad \sigma_i^x = 1 - 2c_i^\dagger c_i. \quad (43)$$

Thus the Hamiltonian will be transformed into

$$\mathcal{H}_0 = -J \sum_{i=1}^L \left[ (c_i^\dagger - c_i) (c_{i+1}^\dagger + c_{i+1}) - g (c_i^\dagger - c_i) (c_i^\dagger + c_i) \right]. \quad (44)$$

The dual JW transformation is then given by [41]

$$c_i^\dagger - c_i = -(a_i^\dagger - a_i), \quad c_{i+1}^\dagger + c_{i+1} = a_i^\dagger + a_i, \quad (45)$$

with  $a_j^\dagger$  and  $a_j$  being dual JW fermion creation and annihilation operators, and  $\mathcal{H}_0$  follows

$$\mathcal{H}_0 = 2J \sum_{i=1}^L \left( a_i^\dagger a_i - \frac{1}{2} \right) - Jg \sum_{i=1}^L (a_{i+1}^\dagger - a_{i+1}) (a_i^\dagger + a_i). \quad (46)$$

The corresponding Hilbert space is expressed as a direct sum of the Ramond (R,  $\mathcal{V}_R$ ) and Neveu-Schwarz (NS,  $\mathcal{V}_{NS}$ ) sectors. We introduce the Bogoliubov transformation [56]

$$\gamma_q = u_q a_q - i v_q a_{-q}^\dagger, \quad \gamma_q^\dagger = u_q a_q^\dagger + i v_q a_{-q}, \quad (47)$$

with

$$u_q = \cos \frac{\theta_q}{2}, \quad v_q = \sin \frac{\theta_q}{2}, \quad \tan \theta_q = \frac{g \sin q}{1 - g \cos q}, \quad (48)$$

in particular for  $q = 0$ ,

$$u_q = 1, \quad v_q = 0. \quad (49)$$

$\mathcal{H}_0$  can then be diagonalised as

$$\mathcal{H}_0 = \sum_q \varepsilon_q \left( \gamma_q^\dagger \gamma_q - \frac{1}{2} \right), \quad (50)$$

where

$$\varepsilon_q = 2J \sqrt{1 + g^2 - 2g \cos q}. \quad (51)$$

The eigenvectors in the two subspaces are

$$|P\rangle_R = |p_1, \dots, p_n\rangle_R = \gamma_{p_1}^\dagger \gamma_{p_2}^\dagger \gamma_{p_3}^\dagger \dots \gamma_{p_n}^\dagger |0\rangle_R \in \mathcal{V}_R, \quad (52)$$

$$|Q\rangle_{NS} = |q_1, \dots, q_m\rangle_{NS} = \gamma_{q_1}^\dagger \gamma_{q_2}^\dagger \gamma_{q_3}^\dagger \dots \gamma_{q_m}^\dagger |0\rangle_{NS} \in \mathcal{V}_{NS}, \quad (53)$$

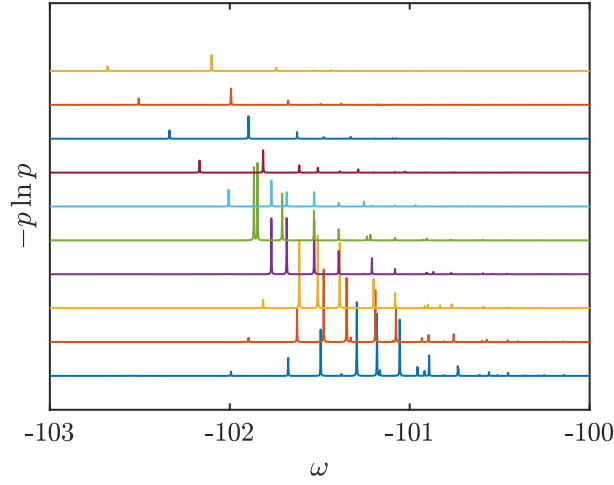


FIG. 4.  $-p \ln p$  vs.  $\omega$  for different  $\kappa$  from 0.2 to 2 with  $\Delta\kappa = 0.2$ , corresponding to the curves from the bottom to the top, after a Lorentzian broadening with  $\alpha = 0.001$ .

with the quantum number  $p$  and  $q$

$$\mathcal{P} : \left\{ p = \frac{2\pi}{L} j \right\}, \quad \mathcal{Q} : \left\{ q = \frac{2\pi}{L} \left( j - \frac{1}{2} \right) \right\}, \quad j = -\frac{L}{2} + 1, -\frac{L}{2} + 2, \dots, \frac{L}{2}. \quad (54)$$

The non-trivial part for the construction of Eq. (41) is given by the FF of  $\sigma^z$  operator, and the FF of  $\sigma_1^z$  follows [41]

$$\begin{aligned} R\langle P | \sigma_1^z | Q \rangle_{NS} &= R\langle p_1, p_2, \dots, p_n | \sigma_1^z | q_1, q_2, \dots, q_m \rangle_{NS} \\ &= \delta_{m-n,0}^{(\text{mod } 2)} i^{-(n+m)/2} (-1)^{n(n-1)/2} \prod_{p \in \mathcal{P}} e^{-ip/2} \prod_{q \in \mathcal{Q}} e^{iq/2} \left( \frac{2}{L} \right)^{(m+n)/2} h^{(m-n)^2/4} \sqrt{\xi \xi_T} \\ &\times \prod_{q \in \mathcal{Q}} \frac{e^{\eta(q)/2}}{\sqrt{\varepsilon_q}} \prod_{p \in \mathcal{P}} \frac{e^{-\eta(p)/2}}{\sqrt{\varepsilon_p}} \prod_{q < q' \in \mathcal{Q}} \frac{4 \sin\left(\frac{q-q'}{2}\right)}{\varepsilon_q + \varepsilon_{q'}} \prod_{p < p' \in \mathcal{P}} \frac{4 \sin\left(\frac{p-p'}{2}\right)}{\varepsilon_p + \varepsilon_{p'}} \prod_{q \in \mathcal{Q}} \prod_{p \in \mathcal{P}} \frac{\varepsilon_q + \varepsilon_p}{4 \sin\left(\frac{q-p}{2}\right)}, \end{aligned} \quad (55)$$

where  $\xi = (1 - g^2)^{1/4}$  and

$$\xi_T = \frac{\prod_{q \in \mathcal{Q}} \prod_{p \in \mathcal{P}} (\varepsilon_q + \varepsilon_p)^{1/2}}{\prod_{q, q' \in \mathcal{Q}} (\varepsilon_q + \varepsilon_{q'})^{1/4} \prod_{p, p' \in \mathcal{P}} (\varepsilon_p + \varepsilon_{p'})^{1/4}}, \quad e^{\eta(\alpha)} = \frac{\prod_{q' \in \mathcal{Q}} (\varepsilon_\alpha + \varepsilon_{q'})}{\prod_{p' \in \mathcal{P}} (\varepsilon_\alpha + \varepsilon_{p'})}. \quad (56)$$

The spin operator  $\sigma_1^z$  is then associated with  $\sigma_1^z$  as

$$R\langle P | \sigma_1^z | Q \rangle_{NS} = e^{i(l-1)(\sum_{q \in \mathcal{Q}} q - \sum_{p \in \mathcal{P}} p)} R\langle P | \sigma_1^z | Q \rangle_{NS}. \quad (57)$$

We can then obtain all the matrix elements for Eq. (41). However, due to the exponential growth of the Hilbert space, a truncation of the full Hamiltonian is necessary, which is the key to TLFFA. In this paper, we include only states that satisfy the zero total momentum constraint and have an energy upper bound of  $10J$  [42, 43],

$$\sum_i k_i = 0 \quad \text{and} \quad \sum_{k_i} \varepsilon_{k_i} \leq 10J. \quad (58)$$

## F. LE spectrum

The detailed data for the LE spectral entropy  $S_{LE} = -\sum_n p_n \ln p_n$ , where  $p_n = |\langle \phi_n | \psi_0 \rangle|^2$  are provided. These data were calculated using the TLFFA algorithm with  $L = 80$  and 8192 truncated states for several values of  $\kappa$ . It can be observed that as  $\kappa$  decreases to  $\kappa < 1$ , the number of peaks increases, accompanied by spectral weight growth. This suggests an increase in the LE spectral entropy and, consequently, an enhancement of the many-body Landau-Zener tunneling due to the quantum geometric effects.